On-orbit frequency identification of spacecraft based on attitude maneuver data

Yong Xie, Pan Liu and Guoping Cai
Department of Engineering Mechanics, Shanghai Jiaotong University, Shanghai, China

Abstract

Purpose – The purpose of this paper is to present an on-orbit frequency identification method for spacecraft directly using attitude maneuver data. Natural frequency of flexible solar arrays plays an important role in attitude control design of spacecraft with solar arrays, and its precision will directly affect the accuracy of attitude maneuver. However, when the flexibility of the solar arrays is large, because of air damping, gravity effect etc., the frequency obtained by ground test shows great error compared with the on-orbit real value. One solution to this problem is to conduct on-orbit identification during which proper identification methods are used to obtain the parameters of interest based on the real on-orbit data of spacecraft.

Design/methodology/approach – The observer/Kalman filter identification and eigensystem realization algorithm are used as identification methods, and the attitude maneuver controller is designed using the rigid-body dynamics method.

Findings – Two conclusions are drawn in this paper according to results of numerical simulations. The first one is that the attitude controller based on the rigid-body dynamics method is effective in attitude maneuver of the spacecraft. The second one is that the on-orbit parameter identification can be directly achieved by using attitude maneuver data of spacecraft without adding additional missions.

Practical implications – Based on the methods proposed in this paper, it is convenient to obtain the natural frequencies of the spacecraft using the data of the attitude maneuver, which may greatly reduce the cost of on-orbit identification test.

Originality/value – The way of obtaining natural frequencies based on attitude maneuver data of spacecraft provides high originality and value for practical application.

Keywords Spacecraft, Attitude controller, ERA, OKID, On-orbit identification

Paper type Research paper

Introduction

With the development of the space industry, large and flexible solar arrays have been widely used in space structures, leading to the low and dense frequencies of the system. For such structures, it is difficult to assemble the system on the ground (1g gravity environment), and it is even more difficult to do ground test because of air damping, gravity effect, etc. Moreover, in some cases, experimental apparatus could not meet the experimental requirement in ground test. On the other hand, flexible parameters of spacecraft, especially the natural frequencies of flexible solar arrays, may have a great effect on the attitude control of spacecraft, because these parameters will be used in control design. When the flexibility of the solar arrays is relatively small, the natural frequencies obtained using the ground test could guarantee the accuracy of the attitude control. However, when the flexibility of the solar arrays is large, the frequencies obtained using the ground test are inaccurate, and the precision of the attitude control would drop sharply if these frequencies are applied to the attitude control design. One way to solve this problem is to perform on-orbit identification work during which proper identification methods are used to obtain the parameters of interest based on the real on-orbit data of spacecraft. As the flexible parameters obtained by the on-orbit identification are based on the real vibration of spacecraft in outer space, high attitude control accuracy may be guaranteed using those parameters in control design.

Generally, the parameter identification method includes two aspects: the time domain method and the frequency domain method. The frequency domain method, which was developed earlier, has anti-noise ability but cannot deal with structures with dense frequencies quite well. Modern space structures with large and flexible appendages tend to have dense frequencies. Therefore, the frequency domain method is not suitable for parameter identification of such structures. However, the time domain method can overcome the above disadvantage. For the time domain method, besides the observer/Kalman filter identification (OKID) and eigensystem realization algorithm (ERA) mentioned in this paper, there are some other methods, such as random decrement technique, natural excitation technique, stochastic subspace identification (SSI), etc. These methods have different characteristics. For example, random decrement technique is used to extract free-decay response from random response of system, and SSI is used for parameter identification of system under ambient

The current issue and full text archive of this journal is available on Emerald Insight at: **www.emeraldinsight.com/1748-8842.htm**

Aircraft Engineering and Aerospace Technology
90/1 (2018) 33–42
 [ISSN 1748-8842]
[DOI 10.1108/AEAT-03-2015-0090]

This work is supported by the Natural Science Foundation of China (11132001, 11272202 and 11472171), the Key Scientific Project of Shanghai Municipal Education Commission (14ZZ021) and the Natural Science Foundation of Shanghai (14ZR1421000).

Received 26 March 2015
Revised 1 June 2016
Accepted 3 June 2016

excitation. In addition, the time domain method can acquire the state-space equation of system in time domain, which provides great convenience for control design.

Up to now, few on-orbit identification tests have been done. For example, the on-orbit model identification experiments were done for the Hubble space telescope using the input and output data of the system (Tobin and Greg, 1995). Two on-orbit forcing function tests were conducted shortly after the spacecraft serving mission. The first test was conducted to determine the modal frequencies of interest. The second test was conducted to determine the gain and damping for the spacecraft significant modes. In the International Space Station (ISS), the shuttle booster ignition pulse was used as an excitation to realize on-orbit modal parameter identification test for five times (Mohamed *et al.*, 2003, 2002). The dynamic responses of the Shuttle-ISS mated structure were measured using the Shuttle payload bay video camera photogrammetric system, the internal wireless instrumentation system (IWIS) accelerometers, and the IWIS strain gages. The measured data were processed and analyzed to identify the structural modal parameters, including frequencies, damping and mode shapes. On the Engineering Test Satellite VI, the parameter identification work was finished by NASDA (Isao and Takashi, 1997; Shuichi and Isao, 1999; Yamaguchi *et al.*, 1995; Ishikawa *et al.*, 1995; Kasai *et al.*, 1997). The satellite was excited by its reaction control system, and its modal parameters were identified based on attitude telemetry data form the attitude control system and six paddle accelerometers. On the Mir Space Station, the external excitations used in on-orbit modal experiment included Shuttle and Mir thruster firings; Shuttle-Mir and progress-Mir dockings crew exercise and push offs; and ambient noise during night-to-day and day-to-night orbital transitions (Kim and Bokhour, 1997; Kim and Kaouk, 1998, 1999; NASA, 1996). Those were designed to provide a wide range of load paths, input force levels and frequency contents. The examples above are typical on-orbit identification tests conducted over the past decades. In these tests, space missions are specially designed and performed for on-orbit identification and are extremely costly. In addition, it should be mentioned herein that to obtain the flexible parameters of spacecrafts, the above on-orbit tests are all based on the ERA. This algorithm is a time-domain identification technology that determines the modal parameters only with input-output data of structures. The on-orbit identification needs the excitation data and vibration response of spacecraft. Fortunately, attitude maneuver of spacecraft exactly provides an excitation and the response could be obtained through sensors on the spacecraft. Consequently, we are inspired to consider whether the attitude maneuver data could be directly used for parameter identification. If the data could be used, it would be of great convenience to complete the identification work with the attitude maneuver data without adding additional space missions.

This paper presents a parameter identification method based on the data of attitude maneuver process using a typical spacecraft as research object. The ERA method is adopted here to identify natural frequencies, and the attitude maneuver controller is designed using the rigid-body dynamics method. For the ERA, the existing studies on this method are mostly based on the state information of the system (displacement and velocity) and few are based on the acceleration signal. It is well known that acceleration sensors are widely used in practical engineering, as the acceleration signal of structural response is more realistic and reliable than displacement and velocity signals and is easier to be obtained as well. Therefore, the computational form of ERA method based on acceleration signal is presented in this paper. The effectiveness of the proposed methods is verified by the numerical simulations at the end of this paper. This paper is organized as follows: Section 2 presents the dynamic equation of the spacecraft; the attitude control design for attitude maneuver process is described in Section 3; Section 4 introduces the OKID and the ERA based on the acceleration signal; the numerical simulation results are outlined in Section 5; and Section 6 briefs the conclusions of the research.

Dynamic equation

The spacecraft system adopted in this paper is shown in Figure 1. The system is composed of one rigid body R and two flexible solar arrays $E1$ and $E2$. The two solar arrays are fixed to the rigid body. One side of each solar array is fixed to the rigid body with no displacement and no rotation, and other sides are free. Two acceleration sensors at the end of each solar array are used to measure vibration signals for parameter identification. The $O_b - x_b y_b z_b$ system is the body-fixed base of the system with the point O_b being located on the mass center of the rigid body.

The Lagrange method is adopted to establish the dynamic equation for the spacecraft shown in Figure 1. The detailed process of derivation can be found in studies by Shi (2004) and Jae and Brij (2006). The dynamic equation of the system is (Shi, 2004; Jae and Brij, 2006):

$$\begin{cases} \boldsymbol{J}\dot{\boldsymbol{\omega}}(t) + \tilde{\boldsymbol{\omega}}\boldsymbol{J}\boldsymbol{\omega}(t) + \boldsymbol{N}_1\ddot{\boldsymbol{\eta}}_1(t) + \boldsymbol{N}_2\ddot{\boldsymbol{\eta}}_2(t) = \boldsymbol{u}(t) \\ \ddot{\boldsymbol{\eta}}_1(t) + 2\boldsymbol{\xi}_1\boldsymbol{\Omega}_1\dot{\boldsymbol{\eta}}_1(t) + \boldsymbol{\Omega}_1^2\boldsymbol{\eta}_1(t) + \boldsymbol{N}_1^T\dot{\boldsymbol{\omega}}(t) = \boldsymbol{0} \\ \ddot{\boldsymbol{\eta}}_2(t) + 2\boldsymbol{\xi}_2\boldsymbol{\Omega}_2\dot{\boldsymbol{\eta}}_2(t) + \boldsymbol{\Omega}_2^2\boldsymbol{\eta}_2(t) + \boldsymbol{N}_2^T\dot{\boldsymbol{\omega}}(t) = \boldsymbol{0} \end{cases} \quad (1)$$

where $\boldsymbol{\omega}(t) \in R^{3\times 1}$ is the attitude angular velocity vector of the system; $\boldsymbol{\eta}_1(t) \in R^{r_1\times 1}$ and $\boldsymbol{\eta}_2(t) \in R^{r_2\times 1}$ are the modal coordinate vectors of the two solar arrays, respectively; r_1 and r_2 are the number of truncated modal for the two solar arrays; $\boldsymbol{J} \in R^{3\times 3}$ is the matrix of moment of inertia of the system; $\boldsymbol{N}_1 \in R^{3\times r_1}$ and $\boldsymbol{N}_2 \in R^{3\times r_2}$ are the modal angular momentum coefficient matrices of the two solar arrays, respectively, their detailed expressions can be found in Shi (2004) and Jae and Brij (2006); $\tilde{\boldsymbol{\omega}} \in R^{3\times 3}$ is a skew-symmetric matrix associated with $\boldsymbol{\omega}(t)$, its definition is given by equation (2); $\boldsymbol{\Omega}_1 \in R^{n_1\times r_1}$

Figure 1 Sketch of the spacecraft structure

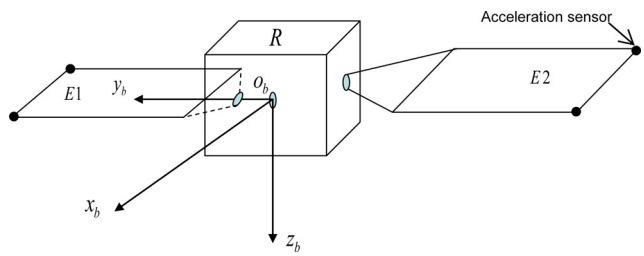

and $\boldsymbol{\Omega}_2 \in R^{r_2 \times r_2}$ are both diagonal matrices with the diagonal elements being the natural frequencies of the two solar arrays, respectively; $\boldsymbol{\xi}_1 \in R^{r_1 \times r_1}$ and $\boldsymbol{\xi}_2 \in R^{r_2 \times r_2}$ are both diagonal matrices with the diagonal elements being the damping ratio of the two solar arrays, respectively; and $\boldsymbol{u}(t) \in R^{3\times 1}$ is the control torque vector acting on the three axes of the rigid body. Throughout the full text, the symbol "$\sim$" denotes a skew symmetric matrix, such as:

$$\widetilde{\boldsymbol{\omega}} = -\widetilde{\boldsymbol{\omega}}^T = \begin{bmatrix} 0 & -\omega_3 & \omega_2 \\ \omega_3 & 0 & -\omega_1 \\ -\omega_2 & \omega_1 & 0 \end{bmatrix}, \ \boldsymbol{\omega} = \begin{bmatrix} \omega_1 \\ \omega_2 \\ \omega_3 \end{bmatrix} \tag{2}$$

Equation (1) can be also written as:

$$\begin{bmatrix} \boldsymbol{J} & \boldsymbol{N}_1 & \boldsymbol{N}_2 \\ \boldsymbol{N}_1^T & \boldsymbol{I}_1 & \boldsymbol{0} \\ \boldsymbol{N}_2^T & \boldsymbol{0} & \boldsymbol{I}_2 \end{bmatrix} \begin{bmatrix} \ddot{\boldsymbol{\theta}}(t) \\ \ddot{\boldsymbol{\eta}}_1(t) \\ \ddot{\boldsymbol{\eta}}_2(t) \end{bmatrix} + \begin{bmatrix} \dot{\tilde{\boldsymbol{\theta}}}\boldsymbol{J} & \boldsymbol{0} & \boldsymbol{0} \\ \boldsymbol{0} & 2\boldsymbol{\xi}_1\boldsymbol{\Omega}_1 & \boldsymbol{0} \\ \boldsymbol{0} & \boldsymbol{0} & 2\boldsymbol{\xi}_2\boldsymbol{\Omega}_2 \end{bmatrix}$$
$$\begin{bmatrix} \dot{\boldsymbol{\theta}}(t) \\ \dot{\boldsymbol{\eta}}_1(t) \\ \dot{\boldsymbol{\eta}}_2(t) \end{bmatrix} + \begin{bmatrix} \boldsymbol{0} & \boldsymbol{0} & \boldsymbol{0} \\ \boldsymbol{0} & \boldsymbol{\Omega}^2 & \boldsymbol{0} \\ \boldsymbol{0} & \boldsymbol{0} & \boldsymbol{\Omega}^2 \end{bmatrix} \begin{bmatrix} \boldsymbol{\theta}(t) \\ \boldsymbol{\eta}_1(t) \\ \boldsymbol{\eta}_2(t) \end{bmatrix} = \begin{bmatrix} \boldsymbol{I} \\ \boldsymbol{0} \\ \boldsymbol{0} \end{bmatrix} \boldsymbol{u}(t) \tag{3}$$

where $\boldsymbol{\theta}(t) = \begin{bmatrix} \theta_1 & \theta_2 & \theta_3 \end{bmatrix}^T \in R^{3\times 1}$ is the attitude angle vector of the system; $\dot{\boldsymbol{\theta}}(t) = \boldsymbol{\omega}(t)$ and $\ddot{\boldsymbol{\theta}}(t) = \dot{\boldsymbol{\omega}}(t)$; and $\boldsymbol{I}_1 \in R^{r_1 \times r_1}$, $\boldsymbol{I}_2 \in R^{r_2 \times r_2}$ and $\boldsymbol{I} \in R^{3\times 3}$ are unit matrices.

Defining a generalized coordinate vector as $\boldsymbol{v}(t) = \left[\boldsymbol{\theta}^T(t), \boldsymbol{\eta}_1^T(t), \boldsymbol{\eta}_2^T(t)\right]^T \in R^{n\times 1}$, $n = 3 + r_1 + r_2$, equation (3) becomes:

$$\boldsymbol{M}\ddot{\boldsymbol{v}}(t) + \boldsymbol{D}_p\dot{\boldsymbol{v}}(t) + \boldsymbol{K}\boldsymbol{v}(t) = \boldsymbol{Q}\boldsymbol{u}(t) \tag{4}$$

where:

$$\boldsymbol{M} = \begin{bmatrix} \boldsymbol{J} & \boldsymbol{N}_1 & \boldsymbol{N}_2 \\ \boldsymbol{N}_1^T & \boldsymbol{I}_1 & \boldsymbol{0} \\ \boldsymbol{N}_2^T & \boldsymbol{0} & \boldsymbol{I}_2 \end{bmatrix}, \ \boldsymbol{D}_p = \begin{bmatrix} \dot{\tilde{\boldsymbol{\theta}}}\boldsymbol{J} & \boldsymbol{0} & \boldsymbol{0} \\ \boldsymbol{0} & 2\boldsymbol{\xi}_1\boldsymbol{\Omega}_1 & \boldsymbol{0} \\ \boldsymbol{0} & \boldsymbol{0} & 2\boldsymbol{\xi}_2\boldsymbol{\Omega}_2 \end{bmatrix},$$
$$\boldsymbol{K} = \begin{bmatrix} \boldsymbol{0} & \boldsymbol{0} & \boldsymbol{0} \\ \boldsymbol{0} & \boldsymbol{\Omega}_1^2 & \boldsymbol{0} \\ \boldsymbol{0} & \boldsymbol{0} & \boldsymbol{\Omega}_2^2 \end{bmatrix}, \ \boldsymbol{Q} = \begin{bmatrix} \boldsymbol{I} \\ \boldsymbol{0} \\ \boldsymbol{0} \end{bmatrix}$$

Attitude control design

Attitude control design for the spacecraft is discussed in this section. Attitude control is one of the most critical aspects of spacecraft design. Put simply, attitude control is a process by which a spacecraft determines and manipulates its orientation relative to other objects or inertial space. The attitude control requirements are determined by the spacecraft's mission. For example, a communication spacecraft must point its antennas toward Earth, its solar arrays toward the sun and its thermal radiators away from the sun. The spacecraft is a non-rooted dynamic system consisting of rigid body and flexible solar arrays. During attitude maneuver, the vibration of the solar arrays will have a negative impact on the accuracy of attitude control. Practically, to reduce or eliminate such influence, the solar arrays are adjusted to parallel the rotating axis of attitude maneuver. In this way, the moment of inertia of the solar arrays relative to the rotating axis would be very great so that the spacecraft can be viewed as a rigid body. Under this circumstance, the attitude controller could be designed by rigid-body dynamic equation, and this design method has great applications in practical engineering as it is simple and easy to implement (Zhou *et al.*, 2006; Wie *et al.*, 1989; Christopher, 2011; Reijneveld and Choukroun, 2012; Srinath *et al.*, 2012). Furthermore, there are two other reasons for the design of attitude controller using rigid-body dynamics method. One reason is that the attitude maneuver proceeds slowly so that the vibration of the solar arrays is relatively small and the negative impact of the solar arrays could be neglected. For this reason, the spacecraft can be regarded as a rigid body system. The other reason is that the attitude controller designed for spacecraft must be simple and practical. Once the vibration of the solar arrays is considered in control design, the attitude controller is bound to become more complex, which would not only increase the cost of the spacecraft but also make the control procedure unstable because of uncertain factors of the system.

In this paper, the rigid-body dynamics method is applied to the design of attitude controller, and the effectiveness of this controller would be testified through numerical simulations.

Attitude kinematics equation

Attitude kinematics equation of spacecraft mainly describes the relation between angular velocity and attitude angle for the spacecraft. The attitude kinematics of spacecraft can be described using Euler rotation angles or attitude quaternion. The kinematics equation for Euler angles involves nonlinear and computationally expensive trigonometric functions, whereas the attitude quaternion-based approach requires less computing time, gives better accuracy and avoids the singularity problems inherent in using Euler rotation angles. Therefore, the quaternion based method is applied to describe the spacecraft attitude in this paper. The spacecraft attitude is determined by its quaternion, defined as (Zhou *et al.*, 2006):

$$\boldsymbol{q} = \begin{bmatrix} q_0 & \overline{\boldsymbol{q}}^T \end{bmatrix}^T = \begin{bmatrix} q_0 & q_1 & q_2 & q_3 \end{bmatrix}^T \in R^{4\times 1} \tag{5}$$

where q_0 and $\bar{q}$ are:

$$q_0 = \cos(\phi/2), \ \overline{\boldsymbol{q}} = \begin{bmatrix} q_1 \\ q_2 \\ q_3 \end{bmatrix} = \begin{bmatrix} e_1\sin(\phi/2) \\ e_2\sin(\phi/2) \\ e_3\sin(\phi/2) \end{bmatrix} \in R^{3\times 1} \tag{6}$$

where ϕ is the magnitude of the Euler axis rotation; and e_1, e_2, and e_3 are the direction cosines of the Euler axis relative to a reference frame.

The kinematics equation of spacecraft described using the quaternion may be written as (Zhou *et al.*, 2006):

$$\begin{cases} \dot{q}_0 = -\dfrac{1}{2}\overline{\boldsymbol{q}}^T\boldsymbol{\omega} \\ \dot{\overline{\boldsymbol{q}}} = \dfrac{1}{2}\left(\widetilde{\overline{\boldsymbol{q}}} + q_0\boldsymbol{I}\right)\boldsymbol{\omega} \end{cases} \tag{7}$$

where $\boldsymbol{\omega} \in R^{3\times 1}$ is the angular velocity vector of the spacecraft; and $\widetilde{\overline{\boldsymbol{q}}}$ is the skew-symmetric matrix associated with $\overline{\boldsymbol{q}}$, and its definition can be found in equation (2).

Attitude controller design

The flexibility of the solar arrays is not considered in this section. It is assumed that O_b-$x_dy_dz_d$ is the desired reference frame of the spacecraft, and the desired attitude of the spacecraft is expressed in O_b-$x_dy_dz_d$. The desired attitude quaternion is defined as:

$$\boldsymbol{q}_d = \begin{bmatrix} q_{d0} & \overline{\boldsymbol{q}}_d^T \end{bmatrix}^T = \begin{bmatrix} q_{d0} & q_{d1} & q_{d2} & q_{d3} \end{bmatrix}^T \in R^{4\times 1} \tag{8}$$

where $\overline{\boldsymbol{q}}_d = \begin{bmatrix} q_{d1} & q_{d2} & q_{d3} \end{bmatrix}^T \in R^{3\times 1}$. The current reference frame is O_b-$x_by_bz_b$, and the current attitude quaternion of the spacecraft is:

$$\boldsymbol{q}_b = \begin{bmatrix} q_{b0} & \overline{\boldsymbol{q}}_b^T \end{bmatrix}^T = \begin{bmatrix} q_{b0} & q_{b1} & q_{b2} & q_{b3} \end{bmatrix}^T \in R^{4\times 1} \tag{9}$$

where $\overline{\boldsymbol{q}}_b = \begin{bmatrix} q_{b1} & q_{b2} & q_{b3} \end{bmatrix}^T \in R^{3\times 1}$. The error quaternion from the current attitude quaternion to the desired one can be expressed as (Srinath *et al.*, 2012):

$$\begin{cases} q_{e0} = q_{b0}q_{d0} + \overline{\boldsymbol{q}}_b^T\overline{\boldsymbol{q}}_d \\ \overline{\boldsymbol{q}}_e = q_{d0}\overline{\boldsymbol{q}}_b - q_{b0}\overline{\boldsymbol{q}}_d - \widetilde{\overline{\boldsymbol{q}}}_d\,\overline{\boldsymbol{q}}_b \end{cases} \tag{10}$$

where $\widetilde{\overline{\boldsymbol{q}}}_d \in R^{3\times 3}$ is the skew-symmetric matrix associated with $\overline{\boldsymbol{q}}_d$.

The error angular velocity vector $\boldsymbol{\omega}_e$ is defined as (Srinath *et al.*, 2012):

$$\boldsymbol{\omega}_e = \boldsymbol{\omega}_b - \boldsymbol{A}_{bd}\boldsymbol{\omega}_d \tag{11}$$

where $\boldsymbol{\omega}_d \in R^{3\times 1}$ and $\boldsymbol{\omega}_b \in R^{3\times 1}$ are the desired and current angular velocity vectors of the spacecraft, respectively; and $\boldsymbol{A}_{bd} \in R^{3\times 3}$ is the direction cosine matrix from O_b-$x_dy_dz_d$ to O_b-$x_by_bz_b$, given by:

$$\boldsymbol{A}_{bd} = \left(q_{e0}^2 - \overline{\boldsymbol{q}}_e^T\overline{\boldsymbol{q}}_e\right)\boldsymbol{I} + 2\overline{\boldsymbol{q}}_e\overline{\boldsymbol{q}}_e^T - 2q_{e0}\widetilde{\overline{\boldsymbol{q}}}_e \tag{12}$$

where $\widetilde{\overline{\boldsymbol{q}}}_e \in R^{3\times 3}$ is the skew-symmetric matrix associated with $\overline{\boldsymbol{q}}_e$.

The error kinematics equation of the spacecraft based on the error quaternion may be written as (Srinath *et al.*, 2012):

$$\begin{cases} \dot{q}_{e0} = -\dfrac{\overline{\boldsymbol{q}}_e^T\boldsymbol{\omega}_e}{2} \\ \dot{\overline{\boldsymbol{q}}}_e = \dfrac{\left(\widetilde{\overline{\boldsymbol{q}}}_e + q_{e0}\boldsymbol{I}\right)\boldsymbol{\omega}_e}{2} \end{cases} \tag{13}$$

The design of attitude controller is presented below. The goal of attitude control is to design a controller satisfying the following expressions:

$$\lim_{t\to\infty}\overline{\boldsymbol{q}}_e = \boldsymbol{0},\ \lim_{t\to\infty}\boldsymbol{\omega}_e = \boldsymbol{0} \tag{14}$$

where $\boldsymbol{0} \in R^{3\times 1}$ is zero vector. From equation (11), one could have:

$$\boldsymbol{\omega}_b = \boldsymbol{\omega}_e + \boldsymbol{A}_{bd}\boldsymbol{\omega}_d \tag{15}$$

By the derivative of equation (15), one can obtain:

$$\dot{\boldsymbol{\omega}}_b = \dot{\boldsymbol{\omega}}_e - \widetilde{\boldsymbol{\omega}}_e\boldsymbol{A}_{bd}\boldsymbol{\omega}_d + \boldsymbol{A}_{bd}\dot{\boldsymbol{\omega}}_d \tag{16}$$

where $\widetilde{\boldsymbol{\omega}}_e$ is the skew-symmetric matrix associated with $\boldsymbol{\omega}_e$.

Omitting the modal vibration equation of the solar arrays in equation (1), the rigid-body dynamic equation can be written as (Wie *et al.*, 1989):

$$\boldsymbol{J}\dot{\boldsymbol{\omega}}_b + \widetilde{\boldsymbol{\omega}}_b\boldsymbol{J}\boldsymbol{\omega}_b = \boldsymbol{u} \tag{17}$$

Substituting equation (16) into equation (17), one can obtain:

$$\boldsymbol{J}\dot{\boldsymbol{\omega}}_e = \boldsymbol{u} - \widetilde{\boldsymbol{\omega}}_b\boldsymbol{J}\boldsymbol{\omega}_b - \boldsymbol{J}(\boldsymbol{A}_{bd}\dot{\boldsymbol{\omega}}_d - \widetilde{\boldsymbol{\omega}}_e\boldsymbol{A}_{bd}\boldsymbol{\omega}_d) \tag{18}$$

The attitude controller adopted in this paper is written as:

$$\boldsymbol{u} = -k_1\overline{\boldsymbol{q}}_e - \boldsymbol{k}_2\boldsymbol{\omega}_e + \widetilde{\boldsymbol{\omega}}_b\boldsymbol{J}\boldsymbol{\omega}_b + \boldsymbol{J}(\boldsymbol{A}_{bd}\dot{\boldsymbol{\omega}}_d - \widetilde{\boldsymbol{\omega}}_e\boldsymbol{A}_{bd}\boldsymbol{\omega}_d) \tag{19}$$

where $k_1 > 0$ is a positive constant and $\boldsymbol{k}_2 \in R^{3\times 3}$ is a positive definite matrix.

Here the Lyapunov method is used to prove that the attitude controller given by equation (19) can stabilize the attitude of the spacecraft globally and asymptotically.

Substituting equation (19) into equation (18), we get:

$$\boldsymbol{J}\dot{\boldsymbol{\omega}}_e = -k_1\overline{\boldsymbol{q}}_e - \boldsymbol{k}_2\boldsymbol{\omega}_e \tag{20}$$

The Lyapunov function is defined as:

$$V_1 = k_1\left[\overline{\boldsymbol{q}}_e^T\overline{\boldsymbol{q}}_e + (q_{e0}-1)^2\right] + \frac{1}{2}\boldsymbol{\omega}_e^T\boldsymbol{J}\boldsymbol{\omega}_e \tag{21}$$

The derivative of V_1 is:

$$\dot{V}_1 = \boldsymbol{\omega}_e^T\boldsymbol{J}\dot{\boldsymbol{\omega}}_e + 2k_1\overline{\boldsymbol{q}}_e^T\dot{\overline{\boldsymbol{q}}}_e + 2k_1q_{e0}\dot{q}_{e0} - 2k_1\dot{q}_{e0} \tag{22}$$

Substituting equation (20) into equation (22) and considering the equations $\overline{\boldsymbol{q}}_e^T\dot{\overline{\boldsymbol{q}}}_e + q_{e0}\dot{q}_{e0} = 0$ and $\dot{q}_{e0} = -\overline{\boldsymbol{q}}_e^T\boldsymbol{\omega}_e/2$, one can get:

$$\dot{V}_1 = -\boldsymbol{\omega}_e^T\boldsymbol{k}_2\boldsymbol{\omega}_e \tag{23}$$

As $\boldsymbol{k}_2$ is a positive definite matrix, one can obtain $\dot{V}_1 \le 0$. Based on the LaSalle invariance principle, one could have:

$$\lim_{t\to+\infty}\boldsymbol{\omega}_e = \lim_{t\to+\infty}\overline{\boldsymbol{q}}_e = \boldsymbol{0} \tag{24}$$

Thus, the attitude controller given in this paper can guarantee that the spacecraft attitude converges to the desired attitude.

On-orbit identification technology

In this section, parameter identification technology will be investigated for the spacecraft. The OKID and ERA will be used in the parameter identification. Both these methods are time-domain identification techniques and have successful applications in practical spacecrafts.

Observer/Kalman filter identification

The OKID is a time-domain identification technique, proposed by Juang et al (1993) and Juang and Phan (2001). It was used to analyze the Hubble Space Telescope after its development. The aim of using the OKID in the parameter identification is to obtain unit impulse response of the system based on the input-output data. Then, ERA can be used to

identify natural frequencies, damping ratio and mode shapes of the system. The OKID has the following characteristics: for a linear time-invariant system, unit impulse response of the system can be obtained using the OKID regardless of the form of external excitation. In other words, the unit impulse response of the system can be obtained using the OKID even if the external excitation of the system is not impulse. Consequently, it becomes possible that on-orbit parameter identification is performed using the attitude maneuver data of the spacecraft. Below, we give detailed calculation format of OKID.

Writing equation (4) into the state equation form and considering the output equation of the system, one could have:

$$\begin{cases} \dot{\boldsymbol{x}}(t) = \boldsymbol{A}_s\boldsymbol{x}(t) + \boldsymbol{B}_s\boldsymbol{u}(t) \\ \boldsymbol{y}(t) = \boldsymbol{C}\boldsymbol{x}(t) + \boldsymbol{D}\boldsymbol{u}(t) \end{cases} \tag{25}$$

where $\boldsymbol{x}(t) = \begin{bmatrix} \dot{\boldsymbol{v}}(t) \\ \boldsymbol{v}(t) \end{bmatrix} \in R^{2n\times 1}$ is the state vector of the system; $\boldsymbol{y} \in R^{l\times 1}$ is the output vector; l is the number of the system output; $\boldsymbol{A}_s = \begin{bmatrix} -\boldsymbol{M}^{-1}\boldsymbol{D}_p & -\boldsymbol{M}^{-1}\boldsymbol{K} \\ \boldsymbol{I} & \boldsymbol{0} \end{bmatrix} \in R^{2n\times 2n}$ and $\boldsymbol{B}_s = \begin{bmatrix} \boldsymbol{M}^{-1}\boldsymbol{Q} \\ \boldsymbol{0} \end{bmatrix} \in R^{2n\times 3}$; and$\boldsymbol{C} \in R^{l\times 2n}$ and $\boldsymbol{D} \in R^{l\times 3}$ are the output and influence matrices, respectively. Here, we discretize equation (25). The analytical solution of the first equation in equation (25) is:

$$\boldsymbol{x}(t) = e^{\boldsymbol{A}_s(t-t_0)}\boldsymbol{x}(t_0) + \int_{t_0}^{t} e^{\boldsymbol{A}_s(t-\tau)}\boldsymbol{B}_s\boldsymbol{u}(\tau)d\tau,\ t \geq t_0 \tag{26}$$

where $\boldsymbol{x}(t_0)$ is the initial value of $\boldsymbol{x}(t)$. Let $t = (k+1)T_s$ and $t_0 = kT_s$ in equation (26), T_s is the data sampling period, we can obtain the following discrete equation:

$$\begin{cases} \boldsymbol{x}(k+1) = \boldsymbol{A}\boldsymbol{x}(k) + \boldsymbol{B}\boldsymbol{u}(k) \\ \boldsymbol{y}(k) = \boldsymbol{C}\boldsymbol{x}(k) + \boldsymbol{D}\boldsymbol{u}(k) \end{cases} \tag{27}$$

where $\boldsymbol{A} = e^{\boldsymbol{A}_sT_s}$ and $\boldsymbol{B} = (\int_0^{T_s} e^{s\boldsymbol{A}_s}ds)\boldsymbol{B}_s$.

From the recursive relations of equation (27), one can obtain the expression of system output at kT_s moment as:

$$\begin{aligned} \boldsymbol{y}(k) &= \boldsymbol{C}\boldsymbol{A}^k\boldsymbol{x}(0) + \sum_{\tau=0}^{k-1}\boldsymbol{C}\boldsymbol{A}^{\tau}\boldsymbol{B}\boldsymbol{u}(k-\tau-1) + \boldsymbol{D}\boldsymbol{u}(k) \\ &= \boldsymbol{C}\boldsymbol{A}^k\boldsymbol{x}(0) + \sum_{\tau=0}^{k-1}\boldsymbol{Y}_{\tau}\boldsymbol{u}(k-\tau-1) + \boldsymbol{D}\boldsymbol{u}(k) \end{aligned} \tag{28}$$

where $\boldsymbol{Y}_{\tau} = \boldsymbol{C}\boldsymbol{A}^{\tau}\boldsymbol{B} \in R^{l\times 3}$ and $\boldsymbol{D}$ are the system Markov parameters to be identified. If the initial condition of the system is zero, the system Markov parameters can be determined directly using equation (28) (Juang *et al.*, 1993). However, for a practical engineering structure, the zero initial condition cannot be exactly guaranteed because there are always certain affecting factors that make the initial condition not exactly be zero. Errors may occur inevitably when the system Markov parameters are identified using equation (28) based on the input-output data of the system. To eliminate the influence of the initial condition on the identification of system Markov parameters, we first construct a state observer whose Markov parameter equation is independent of the initial condition. Then, by solving this equation based on the input-output data to get the observer's parameters and establishing the relationship of Markov parameters between the observer and the original system, we finally work out the Markov parameters of the original system. The detailed process is described below.

Constructing the following state observer (Juang *et al.*, 1993):

$$\begin{cases} \hat{\boldsymbol{x}}(k+1) = \boldsymbol{A}\hat{\boldsymbol{x}}(k) + \boldsymbol{B}\boldsymbol{u}(k) - \boldsymbol{F}\left[\boldsymbol{y}(k) - \hat{\boldsymbol{y}}(k)\right] \\ \qquad\qquad = (\boldsymbol{A} + \boldsymbol{F}\boldsymbol{C})\hat{\boldsymbol{x}}(k) + (\boldsymbol{B} + \boldsymbol{F}\boldsymbol{D})\boldsymbol{u}(k) - \boldsymbol{F}\boldsymbol{y}(k) \\ \hat{\boldsymbol{y}}(k) = \boldsymbol{C}\hat{\boldsymbol{x}}(k) + \boldsymbol{D}\boldsymbol{u}(k) \end{cases} \tag{29}$$

where $\boldsymbol{F} \in R^{2n\times l}$ is the weighting matrix of the observer. The eigenvalues of $\boldsymbol{A} + \boldsymbol{F}\boldsymbol{C}$ are adjusted by the selection of $\boldsymbol{F}$ such that the state $\hat{\boldsymbol{x}}(k) \in R^{2n\times 1}$ of the observer approaches the real state $\boldsymbol{x}(k)$ of the system. The output of the observer at kT_s moment can be written as:

$$\begin{aligned} \hat{\boldsymbol{y}}(k) = \boldsymbol{C}(\boldsymbol{A} + \boldsymbol{F}\boldsymbol{C})^k\hat{\boldsymbol{x}}(0) + \sum_{\tau=0}^{k-1}\hat{\boldsymbol{Y}}_{\tau}\left[\boldsymbol{u}^T(k-\tau-1)\right. \\ \left.\boldsymbol{y}^T(k-\tau-1)\right]^T + \boldsymbol{D}\boldsymbol{u}(k) \end{aligned} \tag{30}$$

where $\hat{\boldsymbol{Y}}_{\tau} \in R^{l\times(l+3)}$ and $\boldsymbol{D}$ are the observer Markov parameters; $\hat{\boldsymbol{Y}}_{\tau}$ is expressed as:

$$\begin{aligned} \hat{\boldsymbol{Y}}_{\tau} &= \left[\boldsymbol{C}(\boldsymbol{A} + \boldsymbol{F}\boldsymbol{C})^{\tau}(\boldsymbol{B} + \boldsymbol{F}\boldsymbol{D}) - \boldsymbol{C}(\boldsymbol{A} + \boldsymbol{F}\boldsymbol{C})^{\tau}\boldsymbol{F}\right] \\ &= \left[\hat{\boldsymbol{Y}}_{\tau}^{(1)} \quad \hat{\boldsymbol{Y}}_{\tau}^{(2)}\right] \end{aligned} \tag{31}$$

where $\hat{\boldsymbol{Y}}_{\tau}^{(1)} = \boldsymbol{C}(\boldsymbol{A} + \boldsymbol{F}\boldsymbol{C})^{\tau}(\boldsymbol{B} + \boldsymbol{F}\boldsymbol{D})$ and $\hat{\boldsymbol{Y}}_{\tau}^{(2)} = -\boldsymbol{C}(\boldsymbol{A} + \boldsymbol{F}\boldsymbol{C})^{\tau}\boldsymbol{F}$.

By selecting $\boldsymbol{F}$ to make the pole of $\boldsymbol{A} + \boldsymbol{F}\boldsymbol{C}$ on the origin, the eigenvalue equation of $\boldsymbol{A} + \boldsymbol{F}\boldsymbol{C}$ will be $(\lambda - \lambda_i)^{2n} = 0$, where λ_i is the ith eigenvalue. Then, by using the Hamilton–Cayley theorem, one can have $(\boldsymbol{A} + \boldsymbol{F}\boldsymbol{C})^{2n} = \boldsymbol{0}$. From equations (27) and (28) and by some derivation, the state error equation can be written as:

$$\boldsymbol{x}(k+1) - \hat{\boldsymbol{x}}(k+1) = (\boldsymbol{A} + \boldsymbol{F}\boldsymbol{C})\left[\boldsymbol{x}(k) - \hat{\boldsymbol{x}}(k)\right] \tag{32}$$

By the recurrence for the state error equation, when $k \geq 2n$, one could have:

$$\begin{aligned} \boldsymbol{x}(k+1) - \hat{\boldsymbol{x}}(k+1) &= (\boldsymbol{A} + \boldsymbol{F}\boldsymbol{C})\left[\boldsymbol{x}(k) - \hat{\boldsymbol{x}}(k)\right] \\ &= (\boldsymbol{A} + \boldsymbol{F}\boldsymbol{C})^2\left[\boldsymbol{x}(k-1) - \hat{\boldsymbol{x}}(k-1)\right] \\ &\vdots \\ &= (\boldsymbol{A} + \boldsymbol{F}\boldsymbol{C})^{2n}\left[\boldsymbol{x}(k-2n+1) - \hat{\boldsymbol{x}}(k-2n+1)\right] \\ &= \boldsymbol{0} \end{aligned} \tag{33}$$

From equation (33), when $k \geq 2n$, the state $\hat{\boldsymbol{x}}(k)$ of the observer will converge to the real state $\boldsymbol{x}(k)$, i.e. $\boldsymbol{x}(k) = \hat{\boldsymbol{x}}(k)$ $(k \geq 2n)$. So, from the second equation of equation (29), the output $\hat{\boldsymbol{y}}(k)$

of the observer will converge to the real output $\boldsymbol{y}(k)$ when $k \geq 2n$, i.e. $\boldsymbol{y}(k) = \widehat{\boldsymbol{y}}(k)$ $(k \geq 2n)$. From equation (31), we know that $\widehat{\boldsymbol{Y}}_\tau = \boldsymbol{0}$ when $\tau \geq 2n$. Therefore, when $k \geq 2n$, equation (30) can be written as:

$$\boldsymbol{y}(k) = \sum_{\tau=0}^{2n-1} \widehat{\boldsymbol{Y}}_\tau \left[\boldsymbol{u}^T(k-\tau-1) \quad \boldsymbol{y}^T(k-\tau-1) \right]^T + \boldsymbol{D}\boldsymbol{u}(k), \qquad k \geq 2n \tag{34}$$

Equation (34) holds strictly and is independent of the initial condition of the system. But equation (30) is subject to the initial condition. Using the least squares to solve equation (34), the Markov parameters $\widehat{\boldsymbol{Y}}_\tau$ and $\boldsymbol{D}$ of the observer can be obtained (Juang *et al.*, 1993). The relationship of Markov parameters between the original system and the observer is (Juang *et al.*, 1993; Juang and Phan, 2001):

$$\boldsymbol{Y}_\tau = \boldsymbol{C}\boldsymbol{A}^\tau\boldsymbol{B} = \widehat{\boldsymbol{Y}}_\tau^{(1)} + \sum_{k=0}^{\tau-1} \widehat{\boldsymbol{Y}}_k^{(2)} \boldsymbol{Y}_{\tau-k-1} + \widehat{\boldsymbol{Y}}_\tau^{(2)} \boldsymbol{D} \tag{35}$$

Based on the input-output data of the system, the Markov parameters of the observer can be obtained from equation (34) and those of the original system can be obtained from equation (35). The natural frequencies of the system can be determined by using the ERA given in the following section. From the above process, it can be observed that the specific value of $\boldsymbol{F}$ is not needed in the entire calculation for Markov parameters.

Eigensystem realization algorithm

ERA is a well-established algorithm for parameter identification in time domain (Juang and Pappa, 1985). It utilizes impulse response data of the system to seek minimal state-space realization by the singular value decomposition of the Hankel block matrix. ERA is established based on the state-space model, and the state vector consists of displacement and velocity. So, the signals of displacement and velocity are more convenient and intuitive for parameter identification (Ha *et al.*, 2015; Zhuo *et al.*, 2004). However, in the on-orbit identification tests that have been carried out in space, acceleration sensors are adopted. Those on-orbit tests indicate that acceleration sensors can be applied to parameter identification of flexible spacecrafts with low and dense frequencies. Here, the ERA in acceleration form is given below (Li, 2007).

When using displacement and velocity as the sensor output and neglecting the influence matrix in the output equation of the system, the state-space form of equation (4) may be written as:

$$\begin{cases} \dot{\boldsymbol{x}}(t) = \boldsymbol{A}_s\boldsymbol{x}(t) + \boldsymbol{B}_s\boldsymbol{u}(t) \\ \boldsymbol{y}_e(t) = \boldsymbol{C}\boldsymbol{x}(t) \end{cases} \tag{36}$$

where $\boldsymbol{y}_e(t)$ is the output vector of displacement and velocity. In a discrete form, equation (36) becomes:

$$\begin{cases} \boldsymbol{x}(k+1) = \boldsymbol{A}_1\boldsymbol{x}(k) + \boldsymbol{B}_1\boldsymbol{u}(k) \\ \boldsymbol{y}_e(k+1) = \boldsymbol{C}\boldsymbol{x}(k+1) \end{cases} \tag{37}$$

where $\boldsymbol{A}_1 = e^{\boldsymbol{A}_s T_s}$ and $\boldsymbol{B}_1 = (\int_0^{T_s} e^{s\boldsymbol{A}_s} ds)\boldsymbol{B}_s$.

When acceleration is used as the sensor output, the state-space equation can be written as:

$$\begin{cases} \dot{\boldsymbol{x}}(t) = \boldsymbol{A}_s\boldsymbol{x}(t) + \boldsymbol{B}_s\boldsymbol{u}(t) \\ \boldsymbol{y}_{ea}(t) = \boldsymbol{C}\dot{\boldsymbol{x}}(t) \end{cases} \tag{38}$$

where $\boldsymbol{y}_{ea}(t)$ is the acceleration output vector. Substituting equation (26) into equation (38) leads to:

$$\dot{\boldsymbol{x}}(t) = \boldsymbol{A}_s \left[e^{\boldsymbol{A}_s(t-t_0)}\boldsymbol{x}(t_0) + \int_{t_0}^{t} e^{\boldsymbol{A}_s(t-\tau)}\boldsymbol{B}_s\boldsymbol{u}(\tau)d\tau \right] + \boldsymbol{B}_s\boldsymbol{u}(t), \quad t \geq t_0 \tag{39}$$

Let $t = (k+1)T_s$ and $t_0 = kT_s$ in equation (39). Then, we can obtain the following discrete equation:

$$\begin{cases} \dot{\boldsymbol{x}}(k+1) = \boldsymbol{A}_2\boldsymbol{x}(k) + \boldsymbol{B}_2\boldsymbol{u}(k) + \boldsymbol{B}_s\boldsymbol{u}(k+1) \\ \boldsymbol{y}_{ea}(k+1) = \boldsymbol{C}\dot{\boldsymbol{x}}(k+1) \end{cases} \tag{40}$$

where $\boldsymbol{A}_2 = \boldsymbol{A}_s e^{\boldsymbol{A}_s T_s} = \boldsymbol{A}_s\boldsymbol{A}_1$ and $\boldsymbol{B}_2 = \boldsymbol{A}_s(\int_0^{T_s} e^{s\boldsymbol{A}_s} ds)\boldsymbol{B}_s = \boldsymbol{A}_s\boldsymbol{B}_1$.

Making the z-transforming for equations (37) and equation (40), one can have:

$$z\boldsymbol{X}(z) = \boldsymbol{A}_1\boldsymbol{X}(z) + \boldsymbol{B}_1\boldsymbol{U}(z) \tag{41}$$

$$z\boldsymbol{Y}_{ea}(z) = \boldsymbol{C}(\boldsymbol{A}_2\boldsymbol{X}(z) + \boldsymbol{B}_2\boldsymbol{U}(z) + \boldsymbol{B}_s z\boldsymbol{U}(z)) \tag{42}$$

where z is the factor of z-transform. From equation (41), one can obtain:

$$\boldsymbol{X}(z) = (z\boldsymbol{I} - \boldsymbol{A}_1)^{-1}\boldsymbol{B}_1\boldsymbol{U}(z) \tag{43}$$

Substituting equation (43) into equation (42), equation (42) is rewritten as follows:

$$\boldsymbol{Y}_{ea}(z) = \left(\boldsymbol{C}\boldsymbol{A}_2 z^{-2}(\boldsymbol{I} - z^{-1}\boldsymbol{A}_1)^{-1}\boldsymbol{B}_1 + z^{-1}\boldsymbol{C}\boldsymbol{B}_2 + \boldsymbol{C}\boldsymbol{B}_s \right)\boldsymbol{U}(z) \tag{44}$$

where $\boldsymbol{U}(z)$ is the system input and $\boldsymbol{Y}_{ea}(z)$ is the system output, so the transfer function $\boldsymbol{H}_t(z)$ can be written as:

$$\boldsymbol{H}_t(z) = \boldsymbol{C}\boldsymbol{A}_2 z^{-2}(\boldsymbol{I} - z^{-1}\boldsymbol{A}_1)^{-1}\boldsymbol{B}_1 + z^{-1}\boldsymbol{C}\boldsymbol{B}_2 + \boldsymbol{C}\boldsymbol{B}_s \tag{45}$$

As:

$$(\boldsymbol{I} - z^{-1}\boldsymbol{A}_1)^{-1} = \sum_{k=0}^{\infty} (z^{-1}\boldsymbol{A}_1)^k = \sum_{k=0}^{\infty} z^{-k}\boldsymbol{A}_1^k \tag{46}$$

Thus, equation (45) becomes:

$$\begin{aligned} \boldsymbol{H}_t(z) &= \boldsymbol{C}\boldsymbol{A}_s\boldsymbol{A}_1 z^{-2}\sum_{k=0}^{\infty} z^{-k}\boldsymbol{A}_1^k\boldsymbol{B}_1 + z^{-1}\boldsymbol{C}\boldsymbol{A}_s\boldsymbol{B}_1 + \boldsymbol{C}\boldsymbol{B}_s \\ &= \boldsymbol{C}\boldsymbol{A}_s\left(\sum_{k=0}^{\infty} z^{-k-2}\boldsymbol{A}_1^{k+1}\boldsymbol{B}_1 + z^{-1}\boldsymbol{B}_1 \right) + \boldsymbol{C}\boldsymbol{B}_s \\ &= \boldsymbol{C}\boldsymbol{A}_s\left(\sum_{k=2}^{\infty} z^{-k}\boldsymbol{A}_1^{k-1}\boldsymbol{B}_1 + z^{-1}\boldsymbol{B}_1 \right) + \boldsymbol{C}\boldsymbol{B}_s \\ &= \boldsymbol{C}\boldsymbol{A}_s\sum_{k=1}^{\infty} z^{-k}\boldsymbol{A}_1^{k-1}\boldsymbol{B}_1 + \boldsymbol{C}\boldsymbol{B}_s \end{aligned} \tag{47}$$

Furthermore, the transfer function of the system in the form of z-transform can also be written as:

$$\boldsymbol{H}_t(z) = \sum_{k=0}^{\infty} \boldsymbol{h}(k) z^{-k} \tag{48}$$

where $\boldsymbol{h}(k) \in R^{l\times 3}$ is the impulse response matrix of the system. Comparing equation (47) with equation (48), one may have:

$$\boldsymbol{h}(0) = \boldsymbol{C}\boldsymbol{B}_s,\ \boldsymbol{h}(k) = \boldsymbol{C}\boldsymbol{A}_s\boldsymbol{A}_1^{k-1}\boldsymbol{B}_1 \tag{49}$$

Next, we use the impulse response matrix to perform parameter identification. The Hankel matrix is constructed as:

$$\overline{\boldsymbol{H}}(k-1) = \begin{bmatrix} \boldsymbol{h}(k) & \boldsymbol{h}(k+1) & \cdots & \boldsymbol{h}(k+\beta-1) \\ \boldsymbol{h}(k+1) & \boldsymbol{h}(k+2) & \cdots & \boldsymbol{h}(k+\beta) \\ \vdots & \vdots & \ddots & \vdots \\ \boldsymbol{h}(k+\alpha-1) & \boldsymbol{h}(k+\alpha) & \cdots & \boldsymbol{h}(k+\alpha+\beta-2) \end{bmatrix} \in R^{\alpha l\times 3\beta} \tag{50}$$

where α and β are the observable and controllable indices, respectively. Substituting equation (49) into equation (50), one can obtain:

$$\overline{\boldsymbol{H}}(k-1) = \boldsymbol{P}_s\boldsymbol{A}_1^{k-1}\boldsymbol{Q}_s \tag{51}$$

where $\boldsymbol{P}_s = \begin{bmatrix} \boldsymbol{C}\boldsymbol{A}_s & \boldsymbol{C}\boldsymbol{A}_s\boldsymbol{A}_1 & \cdots & \boldsymbol{C}\boldsymbol{A}_s\boldsymbol{A}_1^{\alpha-1} \end{bmatrix}^T$ and $\boldsymbol{Q}_s = \begin{bmatrix} \boldsymbol{B}_1 & \boldsymbol{A}_1\boldsymbol{B}_1 & \cdots & \boldsymbol{A}_1^{\beta-1}\boldsymbol{B}_1 \end{bmatrix}$.

Performing the singular value decomposition of $\overline{\boldsymbol{H}}(0)$, one can have:

$$\overline{\boldsymbol{H}}(0) = \overline{\boldsymbol{U}}\boldsymbol{\Sigma}\overline{\boldsymbol{V}}^T \tag{52}$$

where $\boldsymbol{\Sigma} \in R^{2n\times 2n}$ is the singular value diagonal matrix, $\overline{\boldsymbol{U}} \in R^{\alpha l\times 2n}$ is the left singular vector matrix and $\overline{\boldsymbol{V}} \in R^{2n\times 3\beta}$ is the right singular vector matrix.

Based on equation (50), one may observe that:

$$\boldsymbol{h}(k+1) = \boldsymbol{E}_l^T\overline{\boldsymbol{H}}(k)\boldsymbol{E}_3 \tag{53}$$

where $\boldsymbol{E}_l^T = \begin{bmatrix} \boldsymbol{I}_l & \boldsymbol{0}_l & \cdots & \boldsymbol{0}_l \end{bmatrix} \in R^{l\times\alpha l}$; $\boldsymbol{E}_3^T = \begin{bmatrix} \boldsymbol{I}_3 & \boldsymbol{0}_3 & \cdots & \boldsymbol{0}_3 \end{bmatrix} \in R^{3\times 3\beta}$; $\boldsymbol{I}_l \in R^{l\times l}$ and $\boldsymbol{I}_3 \in R^{3\times 3}$ are both unit matrices; and $\boldsymbol{0}_l \in R^{l\times l}$ and $\boldsymbol{0}_3 \in R^{3\times 3}$ are both zero matrices. From Li (2007), one may have:

$$\overline{\boldsymbol{H}}(k) = \overline{\boldsymbol{U}}\boldsymbol{\Sigma}^{1/2}\left(\boldsymbol{\Sigma}^{-1/2}\overline{\boldsymbol{U}}^T\overline{\boldsymbol{H}}(1)\overline{\boldsymbol{V}}\boldsymbol{\Sigma}^{-1/2}\right)^k\boldsymbol{\Sigma}^{1/2}\overline{\boldsymbol{V}}^T \tag{54}$$

Thus, equation (53) can be written as:

$$\boldsymbol{h}(k+1) = \boldsymbol{E}_l^T\overline{\boldsymbol{U}}\boldsymbol{\Sigma}^{1/2}\left(\boldsymbol{\Sigma}^{-1/2}\overline{\boldsymbol{U}}^T\overline{\boldsymbol{H}}(1)\overline{\boldsymbol{V}}\boldsymbol{\Sigma}^{-1/2}\right)^k\boldsymbol{\Sigma}^{1/2}\overline{\boldsymbol{V}}^T\boldsymbol{E}_3 \tag{55}$$

Comparing equation (55) with equation (49), one may derive:

$$\begin{aligned} &\boldsymbol{A}_1 = \boldsymbol{\Sigma}^{-1/2}\overline{\boldsymbol{U}}^T\overline{\boldsymbol{H}}(1)\overline{\boldsymbol{V}}\boldsymbol{\Sigma}^{-1/2},\ \boldsymbol{B}_1 = \boldsymbol{\Sigma}^{1/2}\overline{\boldsymbol{V}}^T\boldsymbol{E}_3, \\ &\boldsymbol{C}\boldsymbol{A}_s = \boldsymbol{E}_l^T\overline{\boldsymbol{U}}\boldsymbol{\Sigma}^{1/2} \end{aligned} \tag{56}$$

Solving the eigenvalues of $\boldsymbol{A}_1$, one can obtain:

$$\boldsymbol{\psi}^{-1}\boldsymbol{A}_1\boldsymbol{\psi} = \boldsymbol{\Lambda},\ \boldsymbol{\Lambda} = diag\left(\overline{\lambda}_1, \overline{\lambda}_2, \cdots, \overline{\lambda}_{2n}\right) \tag{57}$$

where Ψ is the eigenvector matrix of $\boldsymbol{A}_1$ and $\overline{\lambda}_i$ $(i = 1, 2, \ldots, 2n)$ is the ith eigenvalue.

Defining the following variable:

$$f_i = \frac{\ln(\overline{\lambda}_i)}{T_s},\ \ (i = 1,\ 2,\ \cdots,\ 2n) \tag{58}$$

where T_s is the data sampling period. The natural frequency $\hat{\omega}_i$ can be obtained as:

$$\hat{\omega}_i = \sqrt{[\mathrm{Re}(f_i)]^2 + [\mathrm{Im}(f_i)]^2},\ \ (i = 1,\ 2,\ \cdots,\ 2n) \tag{59}$$

where $\mathrm{Re}(f_i)$ and $\mathrm{Im}(f_i)$ are the real part and imaginary part of f_i, respectively.

Numerical simulations

In this section, numerical simulations are carried out to demonstrate the effectiveness of the attitude controller and the identification method proposed in this paper. The spacecraft shown in Figure 1 is used as the object. A flexible plate shown in Figure 2 is adopted to simulate the solar arrays. The left end of the plate is fixed while the right is free. The physical parameters of the plate are listed in Table I. Table II shows the first ten natural frequencies of the plate.

Model reduction and optimal positions of sensors

As we all know, the solar arrays are flexible continuous structures and have infinite degree of freedom. The

Figure 2 Solar array with FEM girding

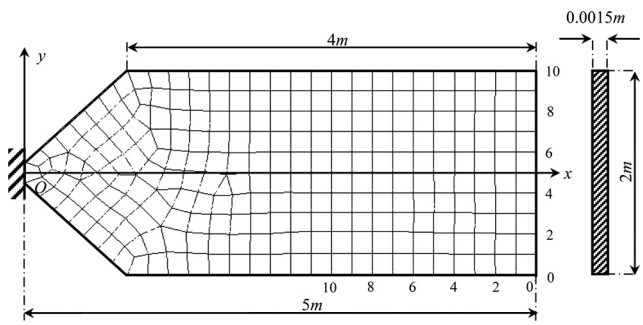

Table I Physical parameters of the solar arrays

Elastic modulus	5×10^{11} Pa	Poisson's rate	0.33
Density	250 kg/m^3	Moment of inertia J_y	31.194 kg·m^2
Mass	3.4125 kg	Moment of inertia J_X	1.0694 kg·m^2

Table II Natural frequency of the solar arrays

Modal order	Frequency (Hz)	Modal order	Frequency (Hz)
1	0.2951	6	11.78
2	1.591	7	13.64
3	2.281	8	18.56
4	5.874	9	19.65
5	6.756	10	22.24

introduction of flexibility brings up a huge challenge to dynamic modeling and control of spacecrafts. Flexible characteristics should be taken into account adequately to exactly describe the dynamic behavior, which results in that the order of dynamic model is often very high. But control design and implementation requires that the order of the system should be as low as possible. Therefore, model reduction should be done so as to obtain a low-order model which is convenient for control design. This low-order model should not only be able to reflect the dynamic characteristics of the original system but also be low enough for the control design and implementation. On the other hand, from the point of dynamic simulation, model order should not be high to improve computing efficiency. For spacecraft system, the common methods for reduction are the inertia complete criterion, modal cost analysis method and balanced truncation technique. In this paper, the inertia complete criterion is used for the model reduction of solar arrays. The inertia complete criterion was proposed by Hughes (Hughes, 1980). The basic idea of this method is determining the number of the modes that contribute most to the completeness of the system. For the solar arrays considered in Figure 2, the proportion of the first ten modal mass in the total modal mass is $\sum_{k=1}^{10} m_k/\overline{m} = 97.137\%$, and proportions of the first ten modal moment of inertia relative to the moment of inertia in x and y directions are $\sum_{k=1}^{10} \mathcal{J}_{xk}/\mathcal{J}_x = 98.986\%$ and $\sum_{k=1}^{10} \mathcal{J}_{yk}/\mathcal{J}_y = 99.704\%$, respectively. It can be observed that it is enough to truncate the first ten modes of the solar arrays. So, the parameters r_1 and r_2 are both chosen to be ten in the numerical simulation.

In the study of parameter identification of this paper, output data of the spacecraft should be obtained through sensor measurement when the spacecraft performs attitude maneuver. It is assumed that two acceleration sensors are used for each solar array, so there are totally four sensors for the spacecraft. However, installation of sensors on the solar arrays is expensive and the number of sensors is limited, so it is expected that the sensors should be installed on the optimal position of the solar arrays. In our study, the optimal positions of the sensors on the solar arrays are determined using the particle swarm optimization (PSO), and the calculation results are shown as the black spots in Figure 1. Those optimal positions are the same as those for the engineering test satellite-VI given by Shuichi and Isao (1999). The calculation process of PSO can be found in studies by Sylvaine *et al.* (2001) and Chen *et al.* (2009).

Attitude control simulation

The performance of the attitude controller given in Section 3.2 is verified through numerical simulations. In the spacecraft maneuver, the spacecraft shown in Figure 1 is required to rotate around the x_b axis from 0 to 45°. The desired trajectories of angular velocity and acceleration are shown in Figure 3. Figure 3 indicates that the system begins to rotate with a uniformly accelerated motion from the zero initial condition. The angular velocity of the system reaches its maximum at 10 s, then the system rotates with a uniform motion in the period of [10 s, 15 s], and finally with a uniformly decelerated motion and the angular velocity drops to zero at 25 s. The attitude controller is required to drive the system to the desired position while the actual angular velocity is close to the desired one as much as possible. In the simulations, the control gains in equation (19) are taken as $k_1 = 4.8$ and $\boldsymbol{k}_2 = 4.8\boldsymbol{J}$, where $\boldsymbol{J} = \begin{bmatrix} 212 & 10 & 12 \\ 10 & 320 & 15 \\ 12 & 15 & 417 \end{bmatrix}$ is the moment of inertia of the system. The simulation results shown in Figure 4 are the time histories of attitude angle, angular velocity and control torque in the x_b direction of the spacecraft, where the dotted line is the actual trajectory and the solid line is the desired one. As the maneuver process is carried out in the x_b direction, the control torques in the y_b and z_b directions are very small and the figures are omitted herein. From Figure 4, it can be observed that the attitude controller given in this paper can drive the spacecraft to the desired position.

Parameter identification simulation

The above simulation results indicate that the spacecraft can effectively converge to the desired trajectory by using the attitude controller given in this paper. The parameter identification of the system is performed here by using the attitude maneuver data. The input of the system is the control torque given in Figure 4(c), and the output is the measurement signal of the four sensors on the solar arrays in the maneuver process.

As shown in Figure 3, there are three periods in the attitude maneuver of the spacecraft, namely, uniformly accelerated

Figure 3 Desired trajectory of the spacecraft

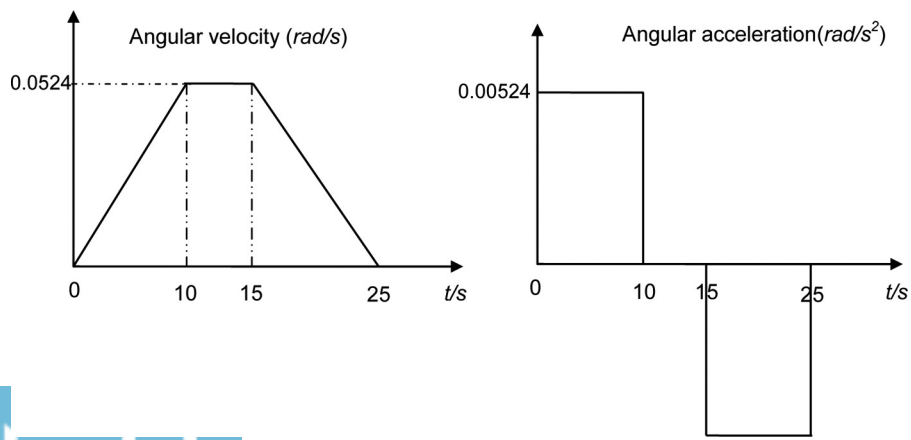

Figure 4 System responses of the spacecraft under control

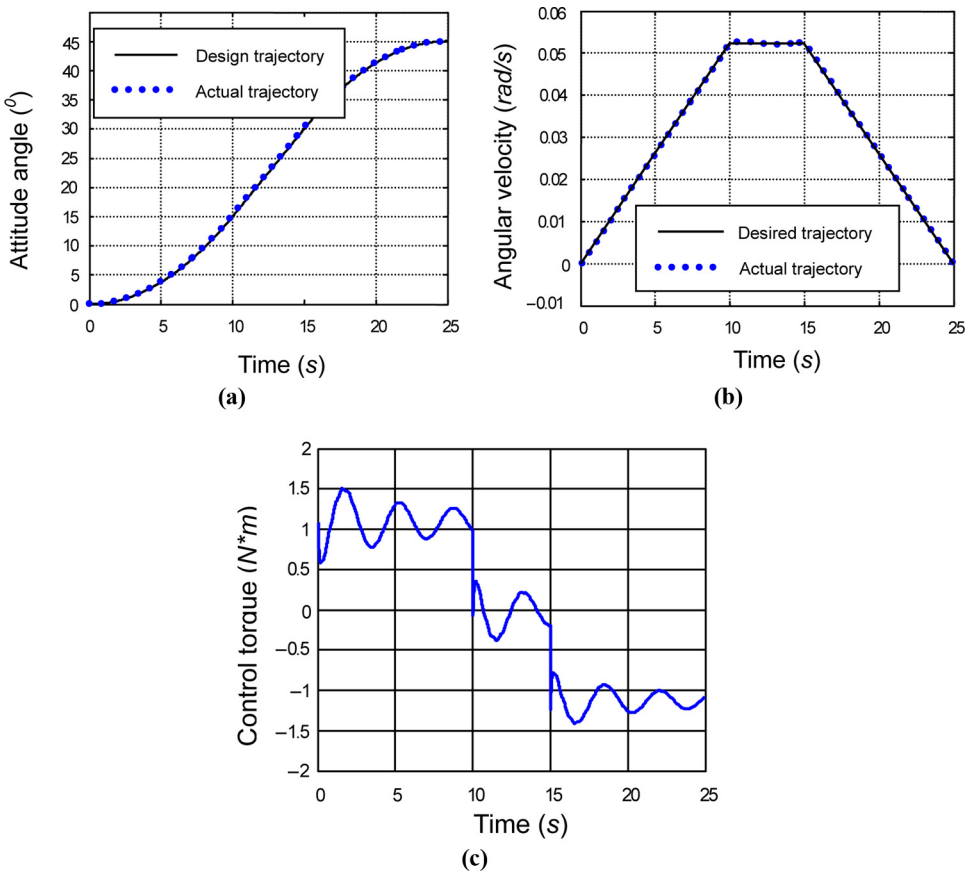

Notes: (a) Attitude angle; (b) angular velocity; (c) control torque

period (0-10 s), uniform velocity period (10-15 s) and uniformly decelerated period (15-25 s). The input and output data in the three periods are independently used for the parameter identification, and the results are displayed in the third, fourth and fifth columns of Table III, respectively. Because the spacecraft shown in Figure 1 is symmetrical, the natural frequencies of the system corresponding to the symmetric and anti-symmetric modes are very close. The theoretical values of natural frequencies are calculated based on equation (4) and are given in the second column of Table III. It can be seen from Table III that the identification results are very close to the theoretical ones, which proves that the on-orbit parameter identification using attitude maneuver data of the spacecraft is feasible. The extensive simulations indicate that the input and output data of the whole period (0-25 s) could also be used for the parameter identification, and the results are almost as accurate as those of simulations conducted here.

Conclusion

In this paper, the on-orbit frequency identification of spacecraft by using attitude maneuver data of the spacecraft is investigated. The attitude controller is designed using the rigid-body dynamics method, and the natural frequencies are identified using AOKID and ERA. Because the OKID can obtain the unit impulse response of the system regardless of the form of external

Table III Identification results of natural frequencies of the spacecraft

Modal order	Natural frequency (*Hz*)			
	Theoretical values	Identification results (0-10 s)	Identification results (10-15 s)	Identification results (15-25 s)
1, 2	0.2951, 0.4284	0.3051, 0.4140	0.2897, 0.4628	0.3031, 0.4679
3, 4	1.5909, 1.5961	1.5906, 1.5937	1.5935, 1.5981	1.5931, 1.5948
5, 6	2.2810, 2.3302	2.3017, 2.3106	2.3134, 2.3146	2.3035, 2.3069
7, 8	5.8744, 5.8750	5.8739, 5.8754	5.8744, 5.8752	5.8734, 5.845
9, 10	6.7563, 6.7851	6.7634, 6.7682	6.7684, 6.7695	6.7694, 6.7701
11, 12	11.7821, 11.7822	11.7541, 11.7581	11.7535, 11.7583	11.7561, 11.7587
13, 14	13.6447, 13.6623	13.6044, 13.6073	13.6059, 13.6072	13.6049, 13.6089

excitation, it provides possibility of performing on-orbit parameter identification by directly using the attitude maneuver data of the spacecraft. Simulation results indicate that the attitude controller given in this paper can drive the spacecraft to the desired position, and the natural frequencies of the spacecraft can be successfully identified using the attitude maneuver data of the spacecraft.

References

Chen, L.X., Cai, G.P. and Pan, J. (2009), "Experimental study of delayed feedback control for a flexible plate", *Journal of Sound and Vibration*, Vol. 322 Nos 4/5, pp. 629-651.

Christopher, M.C. (2011), "Attitude control actuators for a simulated spacecraft", *AIAA Guidance, Navigation, and Control Conference*, Portland, OR, August.

Ha, J., Kang, B., Hong, K. and Oh, S. (2015), "A study on the control method of a ship borne launcher using a system identification method", *19th International Conference on System Theory, Control and Computing (ICSTCC)*, Cheile Gradistei, October, pp. 889-894.

Hughes, P.C. (1980), "Modal identities for elastic bodies with application to vehicle dynamics and control", *Journal of Applied Mechanics*, Vol. 47 No. 1, pp. 177-184.

Isao, Y. and Takashi, K. (1997), "ETS-VI on-orbit system identification experiments", *JSME International Journal*, Vol. 40 No. 4, pp. 623-629.

Ishikawa, S., Yamada, K., Yamaguchi, I. and Chida, Y. (1995), "ETS-VI on-orbit parameter estimation by random excitation", *Proceedings of Astrodynamics Symposium*, Halifax.

Jae, J. and Brij, A. (2006), "Experiments on jerk-limited slew maneuvers of a flexible spacecraft", *AIAA Guidance, Navigation and Control Conference and Exhibit*, Keystone, CO, August, pp. 1-20.

Juang, J.N. and Pappa, R.S. (1985), "An eigensystem realization algorithm for modal parameter identification and modal reduction", *Journal of Guidance, Control and Dynamics*, Vol. 8 No. 5, pp. 620-627.

Juang, J.N. and Phan, M. (2001), *Identification and Control of Mechanical Systems*. Cambridge University Press, New York, NY.

Juang, J.N., Phan, M., Horta, L.G. and Longman, R.W. (1993), "Identification of observer/Kalman filter Markov parameters: theory and experiments", *Journal of Guidance, Control and Dynamics*, Vol. 16 No. 2, pp. 320-329.

Kasai, T., Komatsu, K. and Sano, M. (1997), "Modal parameter identification of controlled flexible structures", *AIAA Journal of Guidance, Control and Dynamics*, Vol. 20 No. 2, pp. 184-186.

Kim, H.M. and Bokhour, E.B. (1997), "Mir structural dynamics experiment: a flight experiment development", *Proceedings of the 38th AIAA SDM Conference*, Kissimmee, FL, April, Paper No. AIAA-97-1169, pp. 577-585.

Kim, H.M. and Kaouk, M. (1998), "Mir structural dynamics experiment: first phase test and data analysis", *Proceedings of the 39th AIAA SDM Conference*, Long Beach, CA, April, Paper No. AIAA-98-1721, pp. 204-212.

Kim, H.M. and Kaouk, M. (1999), "Mir structural dynamics experiment: first test and model refinement", *Proceedings of the 40th SDM Conference*, St. Louis, MO, April, Paper No. AIAA-99-1453.

Li, H.B. (2007), *Model Parameter Identification Technology of Large Engineering Structures*, Beijing Institute of Technology Press, Beijing.

Mohamed, K., Scot, M.N., Sydney, H., Michael, G., Theodore, B., Brian, R.P. and Peart, W. (2003), *Shuttle-ISS Flight-7A on Orbit Test Verification: Pre and Post Flight Analysis, The Society for Experimental Mechanics*, The Boeing Company.

Mohamed, K., Sydney, H., Theodore, B., David, Y., Walter, P., Michael, G. and George, S. (2002), *Modal Analysis and Correlation of International Space Station 4A Mated Configuration*, Society for Experimental Mechanics, The Boeing Company.

Reijneveld, J. and Choukroun, D. (2012), "Attitude control of the Delfi-n3Xt satellite", *AIAA Guidance, Navigation, and Control Conference*, Minneapolis, MN, August.

Shi, G.P. (2004), "The study of model reduction for dynamics of flexible multibody system", M.D. thesis, ZheJiang University of Technology.

Shuichi, A. and Isao, Y. (1999), "On-orbit system identification experiments on engineering test satellite-VI", *Control Engineering Practice*, Vol. 7, pp. 831-841.

Shuttle-Mir Docking Mission 5 (1996), "Structural mathematical models", STS-81, WG-03 Operations and Systems Integration Document, NASA-JSC Document #WG-3/RSC E/NASA/000/3412-5, October.

Srinath, M., Bill, N. and Evgeny, K. (2012), "L1 Adaptive controller for attitude control of multirotors", *AIAA Guidance, Navigation, and Control Conference*, Minneapolis, MN, August.

Sylvaine, L., Hishan, A.K. and Yvan, B. (2001), "Piezoelectric actuators and sensors location for active control of flexible structures", *IEEE Transaction on Instrument and Measurement*, Vol. 50 No. 6, pp. 1577-1582.

Tobin, A. and Greg, A. (1995), "On-orbit modal identification of the Hubble space telescope", *Proceeding of the American Control Conference*, Seattle, WA, pp. 402-406.

Wie, B., Weiss, H. and Arapostathis, A. (1989), "Quaternion feedback regulator for spacecraft eigenaxis rotations", *Journal of Guidance, Control and Dynamics*, Vol. 12 No. 3, pp. 375-380.

Yamaguchi, I., Kida, T. and Kasai, T. (1995), "Experimental demonstration of LSS system identification by eigensystem realization algorithm", *Proceedings of American Control Conference*, Seattle, WA, June, pp. 407-411.

Zhou, L.N., Tang, G.J. and Li, H.Y. (2006), "Feedback control for attitude maneuver based on Matlab/Simulink", *57th International Astronautical Congress*, Valencia, October, pp. 1-9.

Zhuo, Z., Lu, Q.H., Ren, G.X. and Guo, T.N. (2004), "On-orbit identification and vibration control for solar arrays with low and close frequencies", *Engineering Mechanics*, Vol. 21 No. 3, pp. 84-89.

Corresponding author

Guoping Cai can be contacted at: caigp@sjtu.edu.cn